Article

Identification of Receptor Binding to the Biomolecular Corona of Nanoparticles

Sandra Lara, Fatima Alnasser, Ester Polo, David Garry, Maria Cristina Lo Giudice, Delyan R. Hristov, Louise Rocks, Anna Salvati, Yan Yan, and Kenneth A. Dawson

ACS Nano, **Just Accepted Manuscript** • DOI: 10.1021/acsnano.6b07933 • Publication Date (Web): 23 Jan 2017

Identification of Receptor Binding to the Biomolecular Corona of Nanoparticles

Sandra Lara[1†], Fatima Alnasser[1†], Ester Polo[1], David Garry[1], Maria Cristina Lo Giudice[1], Delyan R. Hristov[1], Louise Rocks[1], Anna Salvati[1], Yan Yan[1], Kenneth A. Dawson[1]**

[1]Centre for BioNano Interactions, School of Chemistry and Chemical Biology, University College Dublin, Belfield, Dublin 4, Ireland. [†]These authors contributed equally to this work.

*Corresponding Authors

Email: kenneth.a.dawson@cbni.ucd.ie, yan.yan@cbni.ucd.ie

KEYWORDS: nanoparticle, biomolecular corona, receptor, low-density lipoprotein, epitope, internalization

ABSTRACT

Biomolecules adsorbed on nanoparticles are known to confer a biological identity to nanoparticles, mediating the interactions with cells and biological barriers. However, how these molecules are presented on the particle surface in biological milieu remains unclear. The central aim of this study is to identify key protein recognition motifs and link them to specific cell-receptor interactions. Here we employed an immuno-mapping technique to quantify epitope presentations of two major proteins in the serum corona, low-density lipoprotein and immunoglobulin G. Combining with a purpose-built receptor expression system, we show that both proteins present functional motifs to allow simultaneous recognition by low-density lipoprotein receptor and Fc-gamma receptor I of the corona. Our results suggest that the 'labelling' of nanoparticles by biomolecular adsorption processes allows for multiple pathways in biological processes in which they may be 'mistaken' for endogenous objects, such as lipoproteins, and exogenous ones, such as viral infections.

When the nanoparticle (NP) surface comes in contact with a biological milieu, adsorption processes lead to a surface-assembly of biomolecules derived from the environment, which has been termed 'biomolecular corona'.[1-3] It is now widely acknowledged that sufficiently long-lived ('hard corona') biomolecular motifs presented at the surface would define how a NP first interacts with and is recognised by cells,[4-11] and such interactions likely define many key biological outcomes (*e.g.*, bio-distribution, targeting, and immune responses).[12-25] For example, apolipoproteins and immunoglobulins have been identified in the biomolecular corona of various types of NPs.[3] Their presence has been suggested to promote active processes driven by receptors on the cells of the liver, which leads to liver accumulation of NPs that have commonly observed for many types of NPs.[26] However, so far the identities of the proteins that were tightly bound to an ensemble of NPs have been determined by mass spectrometry analysis of all the proteins extracted from the surface of all the NPs,[3,27] which provides little information on how these proteins are organised and their binding motifs are presented. The lack of molecular details of corona conformation has hindered us to meaningfully determine 'what the cell sees'.[28,29] Now approaches using immuno-probes for detection of specific protein epitopes presented outwards on the NP surface have recently been developed.[30,31] These allow us to seek direct microscopic molecular connections between the biomolecular corona and specific receptors.

Here we present a systematic method to advance such hypotheses by direct investigation of NP-receptor interactions in biological milieu. As one example, a protein corona derived from human serum on 100 nm silica (SiO_2) NPs was chosen as a model. Given the abundance of low-density lipoprotein (LDL) and immunoglobulin G (IgG) in the corona characterised by proteomics analysis, their orientation on the corona was probed by mapping the epitopes of apolipoprotein B-100 (ApoB-100) epitope for LDL and Fc region for IgG. Approximately 60

ApoB-100 binding sites and 180 Fc binding sites per particle were detected in the biomolecular corona derived from 50% human serum by using fluorescence reporter binder (quantum dots (QDs) functionalized with antibodies). Subsequently, we developed a receptor-fusion protein expression system to study specific recognition by LDL receptor (LDLR) and Fc-gamma receptor I (FcγRI) in appropriate biological milieu. We recognize the difficulty of maintaining effective receptor interactions with soluble receptor fragments for most receptors of interest. Thus, the purpose of these receptor fusion systems is to host relevant receptors, in a manner that retains binding capacity, without seeking to re-engineer the host cell, and all of the complexity and uncertainty this entails. As such the readout of specific recognition of biomolecular corona by receptors is an increase of NP uptake when cells express the receptors in comparison to being devoid of the receptors. The presence of free proteins in normal serum is likely to decrease the detection window, as the competition between free proteins and NP-adsorbed protein recognition motifs for specific membrane receptors would only occur in receptor-expressing cells. Therefore, NP uptake was carried out in human serum that was depleted from the free proteins that are binding ligands for a given receptor in this study. Our data have shown that the uptake of NPs is significantly increased in the cells with greatly elevated expression of either LDLR or FcγRI, suggesting that the specific recognition of corona by the both receptors is coexistent. The specificity of the receptor recognition was further confirmed by competition binding of free ligands with increasing concentrations. Taken together, this study has illustrated that biomolecular corona of NPs retain multiple binding motifs, which can be specifically recognised by different receptors potentially with diverse receptor-ligand affinity.

RESULTS AND DISCUSSION

Physiochemical characterization of NPs in biological milieu. For many particle-serum systems the strongly bound hard corona is sufficiently stable so that it is possible to connect the surface expression of surface adsorbed protein epitopes to the cell biological interactions.[32] Thus we first expose 100 nm SiO_2 NPs to different percentage of human serum (*i.e.*, 10%, 30%, and 50%), and isolate the hard corona-NP complexes by centrifugation. Using denaturalized polyacrylamide gel electrophoresis (SDS-PAGE) and mass spectrometry, the irreversibly bound hard corona proteins on SiO_2 NPs were separated, identified, and analysed (Figure 1a-b and Table S1). Lipoproteins and immunoglobulins were found abundant in all coronas with over 10% and 20% of the total corona proteins, respectively. Key examples include LDL and IgG. LDL particles (20 - 30 nm in diameter), containing several thousand of cholesterol, phospholipid, and triglyceride molecules, possess a single copy of ApoB-100, by which interacts with the LDLR.[33-35] IgG, the most abundant type of antibody in the circulation, is consist of four peptide chains. *Via* the Fc region, IgG binds to a family of Fc-gamma receptors (including FcγRI) to mediate various immunological responses (*e.g.*, activation of phagocytes and antibody-dependent cell mediated cytotoxicity).[36] It is unclear if the higher amount of IgG is a consequence of non-specific adsorption or secondary recognition of disrupted corona proteins by blood borne antibodies.

Next, we sought to characterise their physicochemical properties in appropriate biological milieu. In general for nanomaterials, the role of the milieu is critical and cell origin must be matched to the appropriate biological fluid to ensure fidelity of protein recognition.[29] For the following studies, we intend to use LDL as an example to illustrate the concept. Firstly, we re-dispersed the corona-NP complexes in serum depleted of the lipoproteins (lipoprotein depletion in Figure S1), as it is important to examine the particle uptake in milieu in the absence of free

LDL to avoid competitive binding. Subsequently, we characterised the same NP-corona dispersions that used for cell uptake studies with varied serum concentrations and incubation time. Time-resolved differential centrifuge sedimentation (DCS) analyses showed that in 10% delipidised serum there is a degree of instability of the dispersion over some hours, but for both 30% and 50% serum concentrations the dispersions are stable over the lifetime of typical cell uptake experiments (Figure 1c).

For such stable well-defined dispersions we can analyse the epitopes presented at the surface of nanoparticle-corona complexes using immuno-labelling approaches that have the sensitivity to detect 2-4 epitopes per nanoparticle.[37] monoclonal antibody (mAb) that recognises the region of AA 97-526 of ApoB-100, close to the LDLR recognition site, was conjugated to a gold NP (4.5 nm, Figure S2 a-b) or a QD (4 nm, Figure S2 c-d), respectively. After incubation with immuno-gold NP-mAbs, the ApoB-100 epitopes were visualized by transmission electron microscopy (TEM) (Figure 2a and b). To quantitatively detect the epitope presentation in the same conditions as the NPs are exposed to the cells, we employed QD-mAb mapping technique.[38] Firstly, we examined the titration of ApoB-100 epitopes on the coronas formed by exposure of NPs to 10%, 30%, and 50% human serum at 37 °C for 1 h and re-dispersed in PBS. Different numbers of ApoB-100 epitopes were detected on the different coronas, with the 10% serum corona showing the highest number of ApoB-100 epitopes (Figure 2c). Subsequently, we performed the titration curve of QD-mAb probes with the corona-NP complexes that were formed in 50% serum and then re-dispersed in 50% delipidised serum for 1, 4, and 7 h. The three titration-curves showed significant overlapping, suggesting the number of epitopes remains relatively constant throughout the time period (Figure 2d). It is noted that the number of ApoB-100 epitopes reached a plateau of 60 with an increase ratio of the QD-mAb probes to SiO_2 NPs (Figure 2d), which is

similar to the number of ApoB-100 epitopes that was quantified for the same hard corona (*i.e.*, 50% serum corona) re-dispersed in PBS for 1 h (Figure 2c). This further supports the notion that the corona-NP complexes are stable. Taken together, Figure 2 establishes that potential recognition fragment of ApoB-100 is indeed extensively presented at the NP surface in biological milieu. The question is if it is still recognizable by the relevant receptor, LDLR.

Target cells for study of NP-receptor interactions. A straightforward way of detecting specific uptake pathways is to compare the NP uptake kinetics curves (for example using time-resolved flow cytometry) of two identical populations of cells, one of which has many less (or more) receptors of a given type than the other population of cells with other key receptors that can interact with the NPs remaining unchanged.[39] Silencing RNA (siRNA) of the receptors of interest could be used to determine recognition of NPs by decreasing the receptor expression. To explore the siRNA approach, we transfected LDLR siRNA to decrease the endogenous expression of LDLR in A549 human lung epithelial cells (Figure S3). By comparison of particle uptake between LDLR siRNA and scrambled siRNA transfected A549 cells, it has confirmed that LDLR down regulation leads to a decrease of NP uptake (Figure S4). It is worth noting that LDL exists in different forms in serum (*e.g.*, oxidized LDL), and besides LDLR it can be recognised by other receptors, including LOX-1, CD36, and Toll-like receptor 4 (TLR-4).[40,41] A closer analysis has shown that transfection with LDLR siRNA in A549 cells concurrently increased LOX-1 expression (Figure S3), suggesting a high degree of co-regulation of the genes. Given the cross talking between the receptors, it suggests that comparison of reference and silenced cells may not be a reliable approach in this case.

Alternatively, in this study we have developed a receptor-tag fusion protein expression system that can 'host' a range of target receptors in HEK-293T cells (Figure 3). These cells have a very

low endogenous expression level of LDLR, and transfection of LDLR does not appear to co-regulate at gene (or protein) level within the relevant receptor clusters (Figure S5). Crucially, the receptor is fused with HaloTag®, which can then be labelled with a fluorescent HaloTag® ligand, TMR (Figure 3a). This dye labelling serves an intrinsic measure of receptor expression on a cell-by-cell basis using flow cytometry. As it was shown in Figure 3b-c, the expression of LDLR-HaloTag® fusion protein and HaloTag® protein alone varied significantly between cells. Some cells failed to be transfected (the left-most low TMR subpopulation in Figure 3b and c) even with optimisation of the transfection (Figure S6). Hence, we note that if the complete ensemble of cells after transfection is used (both parts of the populations in Figure 3b) it becomes difficult to identify NP-receptor recognition. The correlation between receptor expression level and NP uptake is critical for confirming the specific corona epitope-receptor recognition, given the heterogeneity in both receptor expression and particle-surface presentation. Thus, cell subpopulations (*i.e.*, high TMR and low TMR) were sorted based on TMR intensity. Western blot (Figure 3d) and RT-qPCR (Figure 3e) both confirm that TMR levels can be used as a proxy for receptor expression.

To confirm functionality of the expressed LDLR, we examined the uptake of fluorescently labelled LDL in the high TMR subpopulations (*i.e.*, transfected cells). A four-fold increase in the fluorescence of cells transfected with LDLR was observed compared with the empty vector transfected cells (Figure 3f). It is noted that the LDL uptake was independent of LDLR expression level in the high TMR subpopulation (Figure 3g), suggesting that average numbers of expressed plasma membrane receptors are high and functional.

***In situ* interactions of NPs with LDLR.** Using the above-mentioned LDLR-tag fusion protein expression system, we examined the cell membrane adhesion and uptake of NP-corona in

delipidised serum. For the membrane adhesion experiment, the cells were incubated with NP-corona complexes at 4 °C for 1 and 4 h followed by extensive washes to remove unbound NPs, and subsequently chased in NP-free media at 37 °C for 30 min. For the uptake experiment, the cells were continuously incubated with NP-corona complexes at 37 °C for various time intervals. As shown in Figure 4, significantly increased membrane adhesion and uptake by LDLR-transfected cells (*i.e.*, the high TMR subpopulation) was observed in all dispersions in comparison to cells transfected with empty vector. It is also noted that at higher NP concentration (1mg mL^{-1}) and a higher serum concentration (50% delipidised serum), the specific uptake of NPs by LDLR was maximized, as the baseline uptake (*i.e.*, uptake in cells transfected with empty vector) was minimized due to other uptake pathways suppressed by serum competition (Figure 4 c-d). Under such conditions, the scatter plot (4 h time point as an example) showed a high correlation between LDLR expression and NP uptake on a cell-by-cell basis in the transfected cells (highlighted in the inset box of Figure 4e).

To further establish the specificity of the ApoB-100 interaction we carried out competition uptake experiments (50% delipidised serum, 4 h) for conditions identical to Figure 4c and d, but in the presence of increasing concentrations of fluorescently labelled LDL (Figure 5). Then we can simultaneously measure the uptake of NPs and LDL and find that at around 16 nM LDL here is quite a sharp accumulated displacement-type transition in which predominantly NP uptake crosses over to predominantly LDL uptake (Figure 5a-c). The scatter plot of LDL and NP fluorescence intensity indicates that cells that interact most strongly with LDL also have the highest NP uptake, suggesting involvement of the same receptor (Figure 5d). Confocal microscopy images have also shown a progressive competitive uptake NPs with an increase of free LDL (Figure 5e-g).

We remark that the specific recognition of serum corona by LDLR can be reproduced from independent experiments using the SiO_2 NPs made in house and commercially sourced with the same surface and similar size (Figure S7). Collectively these observations set a high standard of reproducibility, which we find to be broadly applicable to a number of other particle and receptor systems.

Concurrent interactions of NPs with FcγRI receptor. To provide a different perspective, we present (in less detail) analogous data for FcγRI, a receptor that recognises the Fc regions of IgGs, and a member of the important receptor superfamily that promote phagocytosis of (for example) opsonized particles and infectious agents.[42,43] The presentation of Fc epitopes in the biomolecular corona was quantified by using anti-IgG (Fc) QDs labelling. It was shown around 180 Fc epitopes were detected in the corona (Figure 6b), which is higher than the ApoB-100 epitopes (around 60 epitopes) and is consistent with more abundant immunoglobulins found in the corona than apolipoproteins (Figure 1b).

Next, we employed the receptor-tag fusion expression system to examine the specific recognition by FcγRI receptor. As shown in Figure 6c and d, FcγRI-transfected cells exhibited increased uptake of particles compared to untransfected cells in both 30% and 50% IgG-depleted serum, suggesting FcγRI plays a role in particle recognition. The overall uptake scale in IgG-depleted serum is much smaller than that in LDL-depleted serum, despite the fact that abundance of IgG and LDL in the corona and the affinity of free IgG and LDL to FcγRI and LDLR, respectively, are comparable. Also uptake using dual depleted serum (*i.e.* lipid- and IgG-depleted) shows little difference between FcγRI-transfected and control cells (Figure S8) possibly suggesting a much larger interaction between particles and LDLR.[44] The reasons for the apparently less effective interaction of IgG are not clear, and we do not believe it prudent to

over-interpret this observation. We do note, however, that the typical affinities of recognition sites on NPs may be quite unrelated to that of the native protein, and could also vary significantly on a particle-by-particle basis. Such questions go far beyond the current studies, and may require additional tools.

CONCLUSIONS

Fundamentally, the size of NPs moves them into the range where many intrinsic biological messages are passed and processed. Since adsorption of biomolecules on the NPs 'labels' them with endogenous molecules, this potentially allows for ubiquitous 'accidental' involvement in biological processing. Thus, NPs may be 'mistaken' for endogenous (*e.g.*, lipoproteins) or commonly occurring exogenous objects (*e.g.*, viruses), potentially manifested in the nature of their clearance and other outcomes. In this study, by using LDL and IgG as examples we have demonstrated that adsorbed proteins on SiO_2 NPs can present functional epitopes to allow the specific recognition of receptors. While this study has been focused on two types of receptors, we have been able to express a wide spectrum of receptors using such a system (*e.g.*, scavenger receptor class A member 1, scavenger receptor class B member 1, stabilin-1, stabilin-2, and other ten receptors that are abundant in the liver), and consider the platform will be of broad significance for NP-receptor recognition studies.

It would also be important to note that these are only the first steps. There are still several significant limitations that are a consequence of the complexity of NP-cell interactions. For example, NP-protein complexes are highly heterogeneous system in which we have recognized major contributions from predominant, not rare, NP subpopulations. In addition, multivalent interactions between receptors and NPs have often been speculated upon, but the synergies

between receptors at the interface of NPs are poorly studied, and such effects are yet to be understood. Still, we now have systematic mapping and cellular tools that allow us to connect the real nature of the bionanointerface to cellular interactions. This brings closer the microscopic connection between a particle and its biological impacts, with all the promise that could hold for predicting, and controlling, biological outcomes.

METHODS

Materials: Fluorescein isothiocyanate (FITC)-labeled 100 nm SiO_2 NPs with plain surface were synthesized at the CBNI as described previously.[45] 100 nm green fluorescent, plain surface SiO_2 NPs (PSi-G0.1) were purchased from KISKER-BIOTECH (see characterization in Figure S9). Anti-LDL Receptor antibody [1B10H10] (ab204941), Anti-FcγRI antibody [3D3] (ab140779), and Anti-Mouse IgG H&L (HRP) (ab6728) were purchased from Abcam. Anti-ApoB-100 sc-13538, Anti-ApoA-I sc-13549, and Anti-ApoE sc-13521 were purchased from Santacruz Biotech. CD64/FCGR1A Antibody (10.1) MA1-10270 and Goat anti-Mouse IgG (H+L) Secondary Antibody, and Alexa Fluor® 488 conjugate (A11029) were ordered from Thermo Fisher. Human serum (HS) was purchased from BIOCHROM. Delipidised human serum was purchased from SERALAB. IgG-depleted human serum was purchased from INNOV-RESEARCH. The plasmid vectors for expression of LDLR (FHC01394) and FcγRI (FHC03501) were purchased from KAZUSA DNA Research Institute. Quantum™ Simply Cellular® anti-Mouse IgG (BLI815B-5) was ordered from Bangs lab. Propan-2-ol (P/7507/5) was purchased from Fisher Chemical. LDLR Silencer® Select siRNA (s224006), Silencer® Select Negative Control No.1 (439064), and Oligofectamine transfection reagent (12252011) were purchased from Thermo Fisher. Skimmed milk powder (70166), Sodium dodecyl sulfate (L3771), Glycine

(G8898), Ammonium persulfate (A3678), Trizma base (T1503), Tween 20 (P1379), Ethylenediaminetetraacetic acid disodium salt dihydrate, EDTA (E4884), N,N,N′,N′-Tetramethylethylenediamine (T9281), Select Agar (A5054), Acrylamide/bis-acrylamide,40% solution (A7802), Ampicillin (A9393), DL-Dithiothreitol (D5545), Ethanol (32294-2), Methanol (24229-2). 3-Mercaptopropionic acid (M5801), Cadmium chloride (202908), Hydrogen tetrachloroaurate(III) (520918), 4-Aminophenyl β-D-galactopyranoside (A9545), Sodium borhydride (S9125), N-(3-Dimethylaminopropyl)-N′--ethylcarbodiimide hydrochloride (E6383), N-Hydroxysulfosuccinimide sodium salt (56485), Methoxypolyethylene glycol amine (07964)) were purchased from Sigma Aldrich and used as received. Color Plus Pre-stained Protein Ladder, Broad Range (10-230 kDa) (P7711S) and Blue Loading Buffer for SDS-PAGE were purchased from New England Bio-Labs (cat. no. B77035). PVC calibration standard for DCS measurements 483 nm (PS000483) was ordered from Analytik Ltd. BCA Protein Assay Kit (23227) and RIPA buffer (89901) were ordered from Thermo Scientific. Propan-2-ol (P/7507/5) was purchased from Fisher Chemical. Tellurium, 99.8%, Powder (315990250) was purchased from Acros Organics.

NP characterisation: SiO_2 NPs used in this study were characterized by dynamic light scattering (DLS) and DCS to ensure the stability of the dispersion (Figure S9). To obtain hard corona, 1 mg of 100 nm SiO_2 NPs were incubated with 1 mL of 10% human serum (5 mg mL^{-1} protein concentration) or 30% human serum (15 mg mL^{-1} protein concentration) or 50% human serum (25 mg mL^{-1} protein concentration) at 37 °C for 1 h on a shaker followed by centrifugation. 1 mg mL^{-1} of 100 nm SiO_2 NPs were incubated with to allow equilibrium to be reached. Then the samples were centrifuged for 20 min at 16,000 rcf. After centrifugation the pellet was re-dispersed and washes with phosphate-buffered saline (PBS, pH 7.4) for three times.

The protein corona was analysed by SDS-PAGE and electrospray liquid chromatography mass spectrometry (LC-MS/MS) following the protocol described previously.[3] The corona-NP complexes were re-dispersed in 10%, 30% or 50% delipidised human serum, and were characterized by DCS at different time points before the epitope mapping analysis. The NP dispersions were characterized by DCS using a CPS Disc Centrifuge DC24000. DCS measurements were done using a CPS Disc Centrifuge DC24000. For SiO_2 NPs a 8-24% sucrose density gradient (suitable for the nanoparticle density range used) prepared in relevant solvents (PBS, pH 7.4) was used with a disk speed of 20,000 rpm. The particles were measured between 0.001 and 1 μm, each measurement being calibrated with PVC standard of nominal size 483 nm (Analytic Ltd.).

Epitope mapping: The synthesis of small gold NPs (5 nm) was performed following the procedure reported previously.[46] In order to functionalized the gold NPs with antibodies, the citrate of the NP surface was exchanged by a O-(2-Carboxyethyl)-O′-(2-mercaptoethyl) heptaethylene glycol (SH-PEG (7)-COOH, MW= 458.56 g/mol). Briefly, 50 mL of gold NPs after synthesis were incubated overnight, under continuous stirring, with SDS (0.03%), NaOH (25 mM) and an equivalent amount of SH-PEG (7)-COOH to obtain 5,000 chains per NP. The carboxylated gold NPs were washed three times and concentrated with centrifugal filter units (10,000 MWCO). The gold NPs were characterized by DCS and EM. The synthesis of mercaptopropionic acid protected CdTe QDs was performed following the procedure reported by S. Penades *et al*.[47] The QDs were purified by precipitation with acetone. Finally the QDs were separated by centrifugation and dialyzed 48 h against PBS buffer. The QDs particles are characterized by DCS and fluorescence spectroscopy.

The CdTe-MPA QDs and gold NPs were functionalized with antibodies: 1 mL of NP suspension (3.3 nmol) was mixed with 0.4 mg of EDC and 0.8 mg of Sulfo-NHS in PBS buffer pH 7.4, and the mixture was incubated at 37 °C for 30 min. The activated NP solution was applied to a PD-10 column using 10 mM PBS pH 7.4 as the exchange buffer. Then 0.6 nmol of IgG antibody was added to 1 nmol of NPs and the mixture was stirred at 37 °C for 1 h. Subsequently, the activated carboxylic groups were blocked with 5 mg of 4-Aminophenyl β-D-galactopyranoside, and the mixture was incubated overnight in a final volume of 1.5 mL. NPs conjugated with antibodies (650 nM) were stored at 4 °C.

For the immuno-gold labelling, mAb-gold NPs (5 nm) in excess were adding to a given number of corona-NP complexes. After the incubation, the NPs were collected by centrifugation at 16,000 rcf and washes with PBS and milliQ water for 5 times each to remove unbound mAb-gold NPs. And then the samples were prepared for TEM as described previously.[30] A number of 300 SiO_2 NPs were analysed for immuno-gold labelling counting by FEI Tecnai G2 20 Twin TEM operating at accelerating voltage of 200 kV. For the QD-mAbs labelling, different amounts of immuno-QDs in PBS (up to final conc. at 500 nM) were added to the NP-corona complexes (final conc. at 1 mg mL^{-1}) under constant agitation for 1 h at 37 ºC. Subsequently, the samples were centrifuged at 16,000 rcf and re-dispersed in fresh PBS twice to remove the unbound QD-mAbs. The interaction between the immuno-QDs and the corona was studying by steady-state fluorescence spectroscopy as described previously.[31]

Cell culture: Human Embryonic Kidney (HEK-293T) cells were purchased from ATCC (ATCC CRL-3216), which is authenticated by the ATCC. The cells were cultured in DMEM Glutamax (GIBCO), supplemented with 10% Fetal Bovine Serum (FBS, GIBCO) in a humidified chamber at 37 °C under 5% CO_2. Cells were grown in their preferred environment

and passaged three times a week, as they approached 70 - 80% surface coverage. The cells have been routinely tested as mycoplasma contamination free by using MycoAlert Assay kit (Cambrex Bio Science, Nottingham, UK).

RNA extraction and RT-qPCR: RNA was extracted using InviTrap®Spin Cell RNA Mini Kit from Stratec (0711). The amount of RNA was quantified by NanoDrop and the cDNA was obtained by reverse transcription. Quantitative PCR was performed with the cDNA of each population of interest and the specific primers for each receptor. Comparative CT method (ΔΔCT) was used to perform the calculations. The CT (Cycle Treshold) of the receptor of interest was normalized with the CT of the β-actin to obtain its ΔCT. The values of ΔCT of the receptors were further normalized with the ΔCT of the control cells (*i.e.*, untransfected cells), the result of which generated the final data set (ΔΔCT).

Western blot: Proteins separated by SDS-PAGE were transferred to a PVDF membrane using Mini-PROTEAN Tetra Trans-Blot Module under a constant voltage of 100 V for 1 h. Membranes were then incubated at RT for 1 h in blocking solution of 5% skimmed milk in TBS-TWEEN (150 mM NaCl, 10 mM Tris-HCl, 0.1 % Tween, pH 7.5). Afterwards, the membrane was incubated overnight at 4 °C with the antibodies of interest in blocking solution and wash for 1 h in TBS-TWEEN. The blot was incubated at RT for 1 h with 1:2000 of Anti-Goat HRP in blocking solution and washed for 1 h in TBS-TWEEN. The membrane was incubated for 1 min in ECL Western Blotting Substrate mix and visualized in Syngene G: BOX imaging system.

Silencing of LDLR expression in A549 cells: 17,000 cells were seeded in 24-well plates (Greiner), and incubated for 24 h before silencing of LDLR. Cells were then transfected with LDLR siRNA or scrambled siRNA using Oligofectamine reagent according to the manufacturer's instructions, and incubated for 72 h.

Transfection of HEK-293T cells: HEK-293T cells were plated 24 h before transfection at a density of 104,000 cells in each well into a 12-well plate (Cellstar® Greiner bio-one) in 1 mL of completed medium DMEM Glutamax (GIBCO) supplemented with 10% FBS. After 24 h cells were transfected using FuGENE® 6 (Promega)-to-DNA ratio of 3.5:1 for LDLR and 3:1 for FcγRI. Plasmid DNA (0.02 μg μL^{-1}) was added to a sterile tube containing Opti-MEM medium (GIBCO). FuGENE® 6 reagent was added to the solution and mixed carefully by pipetting for 15 times. The solution was incubated at RT for 10 min. 50 μl was then gently added drop wise onto each well and incubated for 24 h at 37 °C and 5% CO_2.

Cellular uptake of NPs: To expose the cells to the NPs, after 24 h of the transfection, cells were washed for at least 30 min in serum-free DMEM. The medium was then replaced by the freshly prepared NP dispersions. Experiments were performed by exposing the cells to the NP dispersions at 0.1 mg mL^{-1} or 1 mg mL^{-1} at 37 °C and 5% CO_2 for 1, 4, and 7 h. Cells then were washed with 1 mL per well of completed DMEM Glutamax supplemented with 10% FBS. One fifth of the volume was replaced with TMR HaloTag® ligand at a concentration of 200 nM in completed DMEM Glutamax, and incubated at 37 °C, 5% CO_2 for 15 min. The cells were washed with completed DMEM Glutamax once and PBS twice, and harvested after trypsinization. Cell pellets were re-dispersed in completed DMEM Glutamax and placed on ice. Cell fluorescence intensity was measured using a CyAn ADP (BECKMAN COULTER Flow Cytometers). Results are reported as the median of cell fluorescence intensity of transfected cells (high TMR subpopulation). At least 15,000 cells were analyzed in each sample.

FIGURES

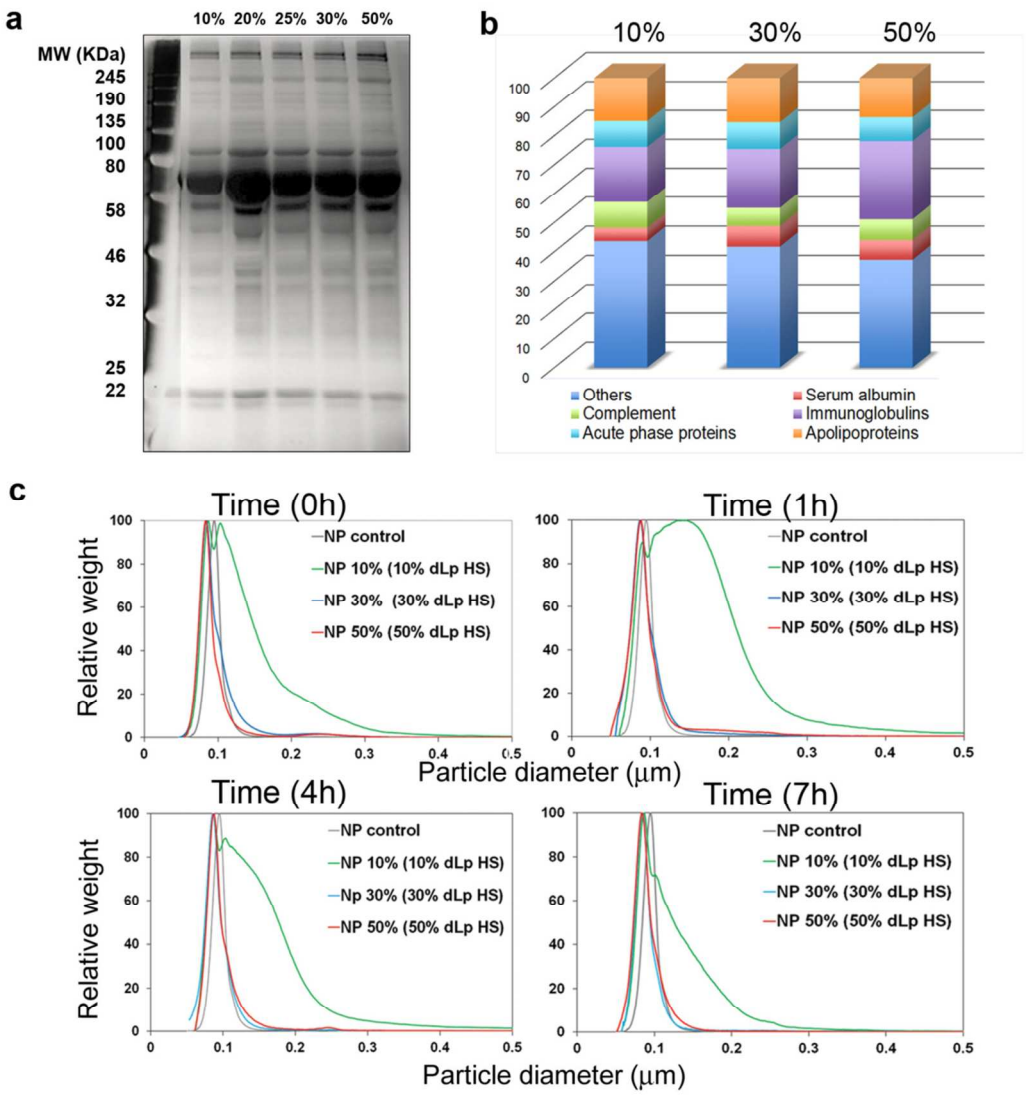

Figure 1. Physicochemical characterization of serum corona on 100 nm SiO_2 NPs. a) SDS-PAGE of protein coronas recovered from SiO_2 NPs following incubation with human serum at various concentrations. b) Distribution of protein groups in human serum corona analyzed by LC-MS/MS. The proteins on the SDS-PAGE were identified by LC-MS/MS after in-gel tryptic digestion. The abundance of protein groups is expressed as protein mass percentage of the total corona proteins. c) DCS analysis of NP dispersions in delipidised human serum for various time

periods: NPs with hard coronas formed in 10%, 30%, and 50% of human serum were re-dispersed in 10%, 30%, and 50% delipidised human serum for 1, 4, and 7 h, respectively.

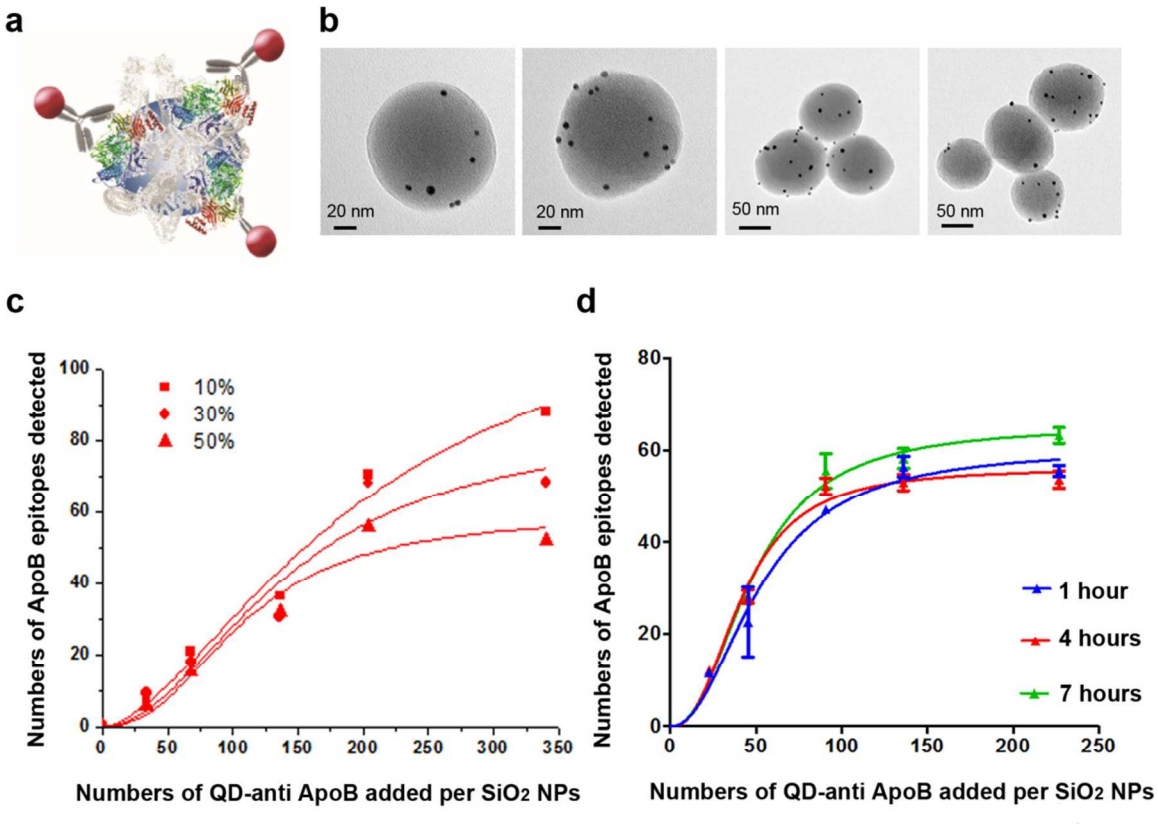

Figure 2. Epitope mapping of ApoB-100 on serum corona of 100 nm SiO_2 NPs. a) Schematic representation of epitope mapping of ApoB-100 on the protein corona of SiO_2 NPs by 5 nm immuno-gold NPs conjugated with antibodies recognizing ApoB-100 epitope. b) EM micrographs of ApoB-100 epitopes on SiO_2 NPs with a corona formed in 50% of human serum and subsequently incubated in 50% of delipidised serum for 4 h. c and d) Quantification of ApoB-100 epitope on corona-NP complexes using immuno-QDs. c) The corona-NP complexes were formed in 10%, 30%, and 50% human serum, and subsequently re-dispersed in PBS for 1 h. The immuno-QDs labelling were performed with the corona-NP dispersion in PBS. d) The corona-NP complexes were formed in 50% human serum, and subsequently re-dispersed in 50% delipidised human serum and incubated for 1, 4, and 7 h. The immuno-QDs were performed with

the corona-NP dispersion in 50% delipidised serum. Data represent the mean and standard deviation of three independent replicates.

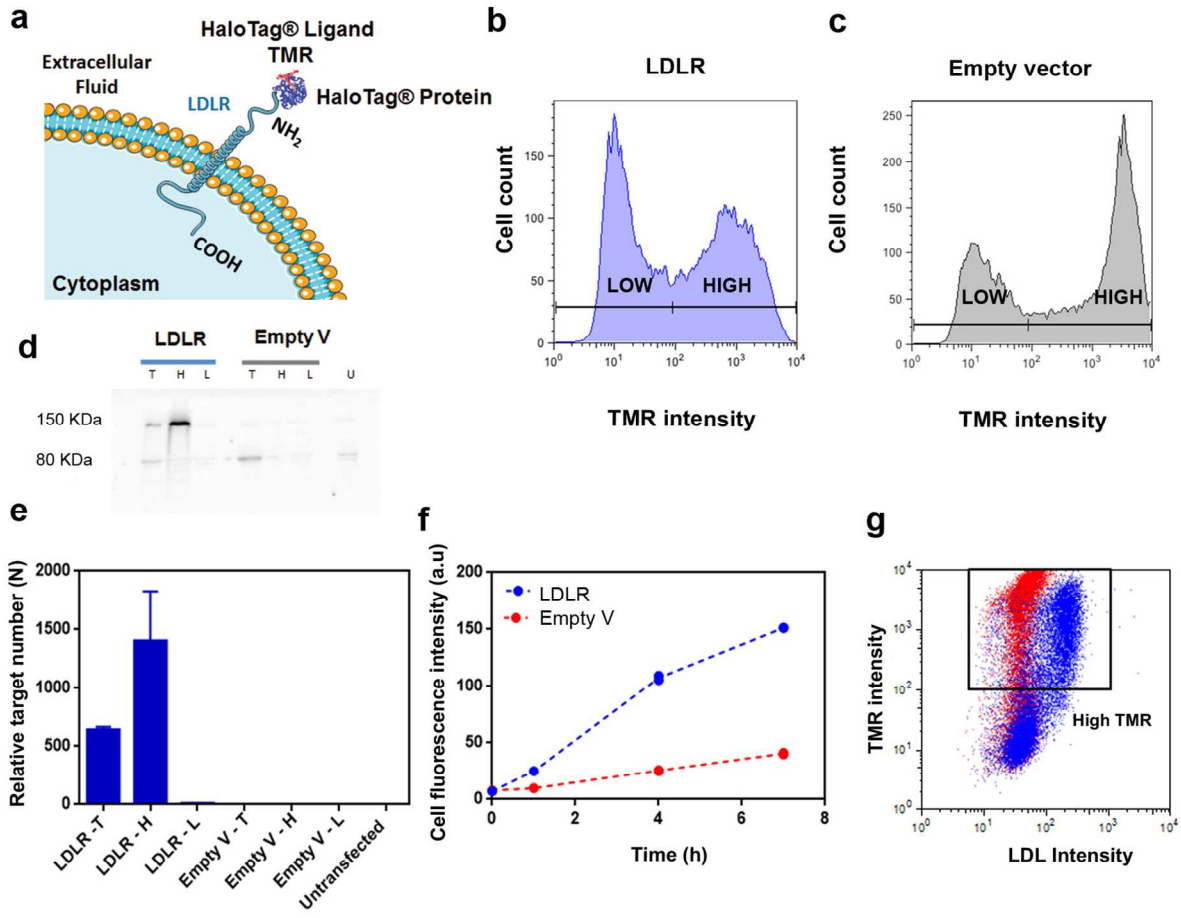

Figure 3. Expression of human LDLR in HEK-293T cells. a) Scheme of LDLR fused with a HaloTag® protein at its N-terminus. The HaloTag® protein forms a covalent bond with a fluorescent HaloTag® ligand, TMR. b) Expression of LDLR-HaloTag® fusion protein in cells transfected with LDLR vector after incubation with TMR measured by flow cytometry. c) Expression of HaloTag® protein in cells transfected with empty vector after incubation with TMR measured by flow cytometry. Cells were sorted to two populations (High and Low) based on the TMR intensity. d) Western blot analysis of LDLR expression (MW 95 KDa) probed by using an anti-LDLR monoclonal antibody. e) Quantification of LDLR mRNA level by RT-qPCR after transfection with LDLR vector in the total cell population (LDLR-T), sorted High TMR (LDLR-H), and Low TMR (LDLR-L) subpopulations, as well as equivalent samples after

transfection with empty vector. The data are shown as the mean ± standard deviation of triplicates. f) Uptake kinetics of BODIPY-LDL (5 μg mL^{-1}) by cells transfected with LDLR vector in 50% human serum analyzed by flow cytometry. Data represent the median fluorescence intensity of transfected cells (high TMR subpopulation) performed in duplicates. At least 15,000 cells were analyzed in each repeat. g) Example of 2D-plot of BODIPY-LDL and TMR intensity (4 h time point). High TMR subpopulation is highlighted in the square. Blue: LDLR-transfected cells. Red: Empty vector transfected cells.

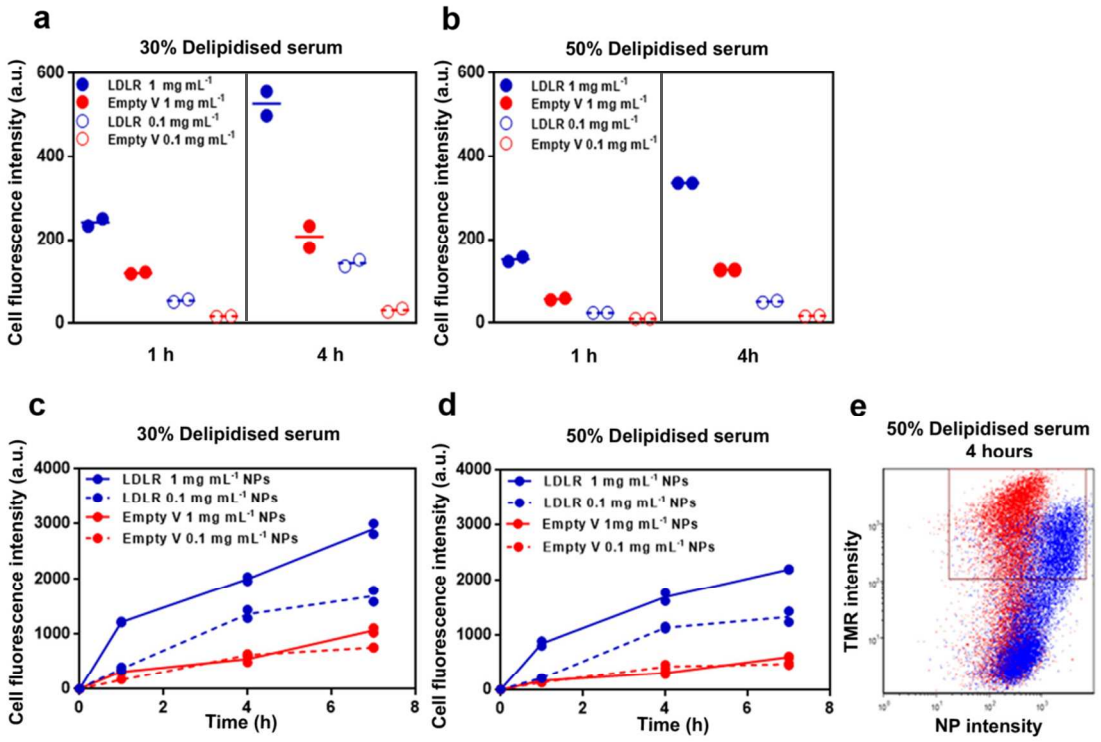

Figure 4. Membrane adhesion and uptake of human serum corona-SiO_2 NP complexes in delipidised serum. a and b) Membrane adhesion of corona-NP complexes in delipidised serum. Cells were exposed to corona-NP complexes in 30% (a) and 50% (b) delipidised serum at 4 °C for 1 h and 4 h, followed incubation at 37 °C for 30 min. Data represent the median fluorescence intensity of transfected cells (high TMR subpopulation) performed in duplicates. At least 15,000 cells in each repeat were measured by flow cytometry. c and d) Uptake of corona-NP complexes in delipidised serum. Cells were exposed to corona-NP complexes in 30% (c) and 50% (d) delipidised serum at 37 °C for 1, 4, and 7 h. Data represent the median fluorescence intensity of transfected cells (high TMR subpopulation) performed in duplicates. At least 15,000 cells were analyzed in each repeat. e) Example of 2D-plot of NP and TMR intensity (50% delipidised serum, 4 h incubation). High TMR subpopulation is highlighted in the square. Blue: LDLR-transfected cells. Red: Empty vector transfected cells.

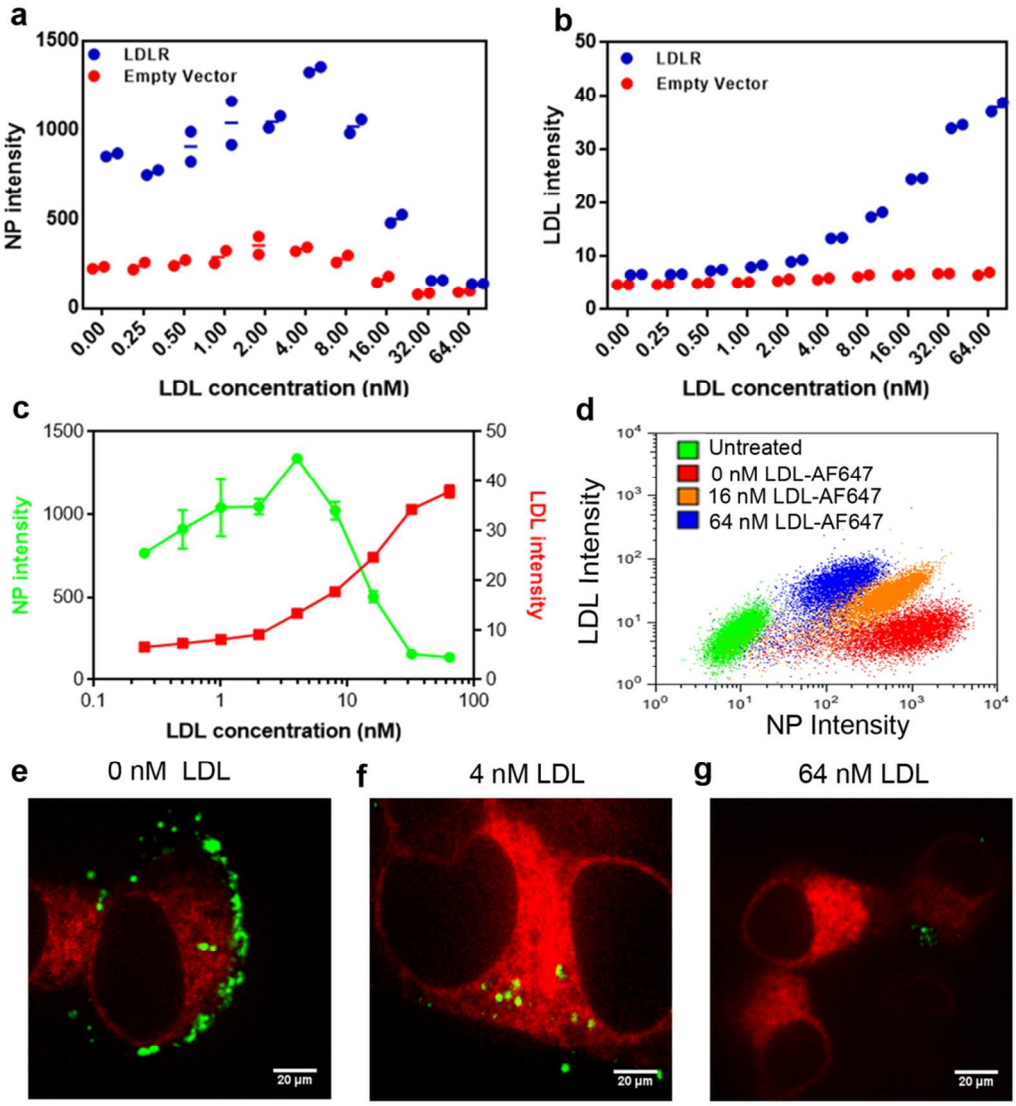

Figure 5. Competitive uptake of human serum corona-SiO_2 NP complexes by LDL in delipidised serum. Cells were incubated with corona- NP complexes (labeled with FITC, 0.1 mg ml-1) and increasing concentrations of AF647-LDL (0 to 64 nM) in 50% delipidised serum at 37 °C for 4 h. NP (a) and LDL (b) uptake were measured by flow cytometry. Data are the median fluorescence intensity of transfected cells (high TMR subpopulation) performed in duplicates. c) Uptake of NPs was competed with LDL in LDLR transfected cells. Data are shown as the mean of cell fluorescence intensity of transfected cells ± standard deviation of duplicates. d) 2D scatter plots show uptake of NPs and LDL in untreated cells, LDLR-transfected cells in the absence and

presence of AF647-LDL. Confocal images of NP uptake (in green) in LDLR-transfected cells (stained with TMR in red) in absence of LDL (e), in the presence of 4 nM LDL (f), and 64 nM LDL (g).

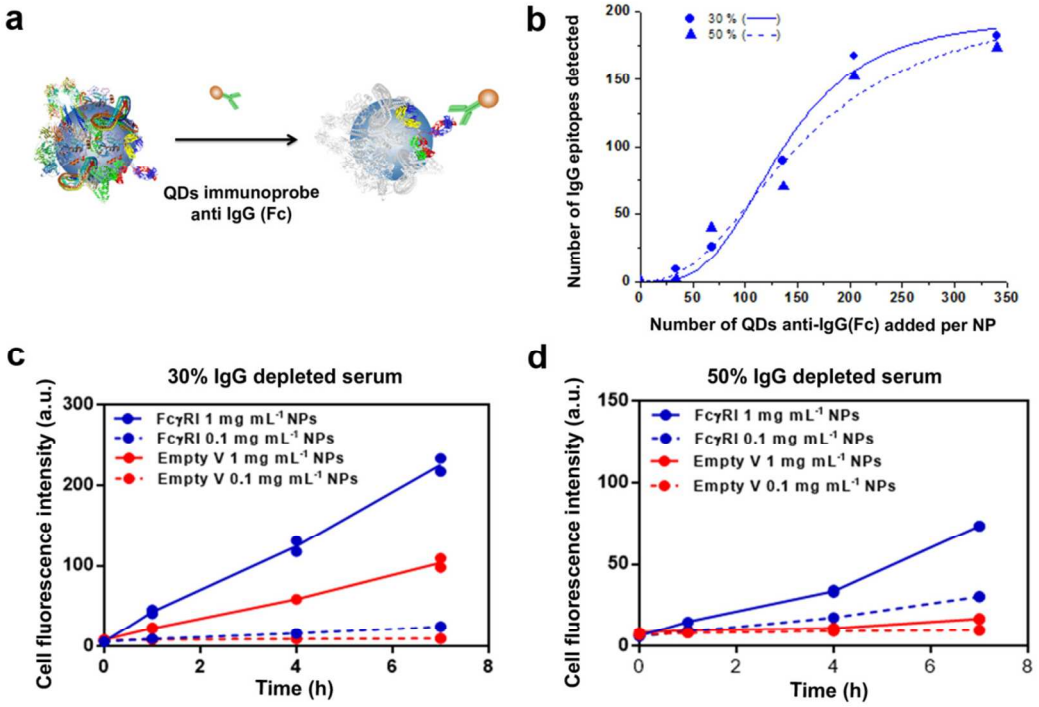

Figure 6. Epitope mapping of IgG (Fc) in serum corona of SiO_2 NPs and their cellular recognition by FcγRI receptor in IgG-depleted serum. a) Schematic representation of epitope mapping of Fc region on the corona of SiO_2 NPs in IgG-depleted serum by immuno-QDs labelling. b) Quantification of Fc epitope on corona-NP complexes using immuno-QDs. The corona-NP complexes were formed in 30% and 50% human serum, and subsequently re-dispersed in PBS for 1 h. The immuno-QDs labelling were measured with the corona-NP dispersion in PBS using fluorescence spectroscopy. c and d) Uptake of corona-NP complexes in IgG-depleted serum. Cells were exposed to corona-NP complexes in 30% (c) and 50% (d) IgG-depleted serum at 37 °C for 1, 4, and 7 h. Data represent the median fluorescence intensity of transfected cells (high TMR subpopulation) performed in duplicates. At least 15,000 cells were analyzed in each repeat.

ASSOCIATED CONTENT

Supporting Information. Table of proteins identified in human serum corona of SiO_2 by LC-MS/MS. Western blot for confirming the depletion of lipids in human serum. Physical characterization of gold NPs and QDs for antibody conjugation. Receptor expression in LDLR-silenced A549 cells. NP uptake in LDLR-silenced A549 cells. Receptor mRNA levels in LDLR-transfected HEK-293T cells. Optimization of transfection. Reproducibility of corona-NP uptake in LDLR-transfected HEK-293T cells. Uptake of corona-NPs in lipid- and IgG-depleted serum. Physicochemical characterization of NPs used in this study. This material is available free of charge *via* the Internet at http://pubs.acs.org.

ACKNOWLEDGMENT

This work was supported by the Science Foundation Ireland (SFI) Principal Investigator Award (Agreement No. 12/IA/1422). S.L., E.P., D.G., M.C.L.G., and L.R. acknowledge the Science Foundation Ireland (SFI, 12/IA/1422). F.A. acknowledges the Saudi Arabia Scholarship Program. Y.Y. acknowledges the EU FP7-PEOPLE-2012-IAPP Marie Curie NanoClassifier (Agreement No. 324519). D.R.H. acknowledges EU FP7 FutureNanoNeeds project (Agreement No. 604602). Experimental method development was also supported by the EU FP7 QualityNano research infrastructure (Agreement No. 2621633). The Conway Institute Flow Cytometry, Biological Imaging Suite, and Proteomics facilities at University College Dublin are also acknowledged. The authors are grateful for assistance from Alfonso Blanco (flow cytometry), Matthias Wilm (proteomics), Kanalaya Prapainop (receptor experiments), Rong Miao (receptor experiments), Andrzej Pitek (receptor experiments), Filippo Bertoli (imaging), and Andre Potti (serum depletion).

REFERENCES

1. Cedervall, T.; Lynch, I.; Lindman, S.; Berggård, T.; Thulin, E.; Nilsson, H.; Dawson, K.A.; Linse, S. Understanding the Nanoparticle–Protein Corona Using Methods to Quantify Exchange Rates and Affinities of Proteins for Nanoparticles. *Proc. Natl. Acad. Sci. U.S.A.* **2007**, *104*, 2050-2055.

2. Monopoli, M.P.; Aberg, C.; Salvati, A; Dawson, K.A. Biomolecular Coronas Provide the Biological Identity of Nanosized materials. *Nat. Nanotechnol.* **2012**, *7*, 779-786.

3. Monopoli, M.P.; Walczyk, D.; Campbell, A.; Elia, G.; Lynch, I.; Bombelli, F.B.; Dawson, K.A. Physical−Chemical Aspects of Protein Corona: Relevance to *in Vitro* and *in Vivo* Biological Impacts of Nanoparticles. *J. Am. Chem. Soc*. **2011**, *133*, 2525-34.

4. Tenzer, S.; Docter, D.; Kuharev, J.; Musyanovych, A.; Fetz, V.; Hecht, R.; Schlenk, F.; Fischer, D.; Kiouptsi, K.; Reinhardt, C.; Landfester, K.; Schild, H.; Maskos, M.; Knauer, S.K.; Stauber, R.H. Rapid Formation of Plasma Protein Corona Critically Affects Nanoparticle Pathophysiology. *Nat. Nanotechnol*. **2013**, *8*, 772-781.

5. Schöttler, S.; Becker, G.; Winzen, S.; Steinbach, T.; Mohr, K.; Landfester, K.; Mailänder, V.; Wurm, F.R. Protein Adsorption Is Required for Stealth Effect of Poly(ethylene glycol)- and Poly(phosphoester)-Coated Nanocarriers. *Nat. Nanotechnol*. **2016**, *11*, 372–377.

6. Deng, Z.J.; Liang, M.; Monteiro, M.; Toth, I.; Minchin, R.F. Nanoparticle-Induced Unfolding of Fibrinogen Promotes Mac-1 Receptor Activation and Inflammation. *Nat. Nanotechnol.* **2011***, 6,* 39-44.

7. Rocker, C.; Potzl, M.; Zhang, F.; Parak, W.J.; Nienhaus, G.U. A Quantitative Fluorescence Study of Protein Monolayer Formation on Colloidal Nanoparticles. *Nat. Nanotechnol*. **2009**, *4*, 577-580.

8. Mortimer, G.M.; Butcher, N.J.; Musumeci, A.W.; Deng, Z.J.; Martin, D.J.; Minchin, R.F; Cryptic Epitopes of Albumin Determine Mononuclear Phagocyte System Clearance of Nanomaterials. *ACS Nano* **2014**, *48*, 3357-3366.

9. Walkey, C.D.; Olsen, J.B.; Guo, H.; Emili, A.; Chan, W.C. Nanoparticle Size and Surface Chemistry Determine Serum Protein Adsorption and Macrophage Uptake. *J. Am. Chem. Soc*. **2012**, *134*, 2139-2147.

10. Del Pino, P.; Pelaz, B.; Zhang, Q.; Maffre, P.; Nienhaus, G.U.; Parak, W.J. Protein Corona Formation around Nanoparticles-from the Past to the Future. *Mater. Horiz.* **2014,** *1*, 301-313.

11. Pelaz, B.; Del Pino, P.; Maffre, P.; Hartmann, R.; Gallego, M.; Rivera-Fernandez, S.; De la Fuente, J.M.; Nienhaus, G.U.; Parak, W.J. Surface Functionalization of Nanoparticles with Polyethylene Glycol: Effects on Protein Adsorption and Cellular Uptake. *ACS Nano*. **2015,** *9*, 6996-7008.

12. He, X.; Zhang, Z.; Liu, J.; Ma, Y.; Zhang, P.; Li, Y.; Wu, Z.; Zhao, Y.; Chai, Z. Quantifying the Biodistribution of Nanoparticles. *Nat. Nanotechnol*. **2011**, *6*, 755.

13. Dobrovolskaia, M.A.; McNeil, S.E. Immunological Properties of Engineered Nanomaterials. *Nat. Nanotechnol*. **2007**, *2*, 469-478.

14. Liang, L.; Li, J.; Li, Q.; Huang, Q.; Shi, J.; Yan, H.; Fan, C. Cover Picture: Single-Particle Tracking and Modulation of Cell Entry Pathways of a Tetrahedral DNA Nanostructure in Live Cells. *Angew. Chem., Int. Ed*. **2014**, *53*, 7745-7750.

15. Kreyling, W.G.; Fertsch-Gapp, S.; Schäffler, M.; Johnston, B.D.; Haberl, N.; Pfeiffer, C.; Diendorf, J.; Schleh, C.; Hirn, S.; Semmler-Behnke, M.; Epple, M.; Parak, W.J. *In Vitro* and *In*

Vivo Interactions of Selected Nanoparticles with Rodent Serum Proteins and Their Consequences in Biokinetics. *Beilstein J. Nanotechnol*. **2014**, *5*, 1699-1711.

16. Hadjidemetriou, M.; Al-Ahmady, Z.S.; Kostarelos, K. Time-Evolution of *In Vivo* Protein Corona onto Blood-Circulating PEGylated Liposomal Doxorubicin (DOXIL) Nanoparticles. *Nanoscale* **2016**, *8*, 6948-6957.

17. Huang, K.; Ma, H.; Liu, J.; Huo, S.; Kumar, A.; Wei, T.; Zhang, X.; Jin, S.; Gan, Y.; Wang, P.C.; He, S.; Zhang, X.; Liang, X.J. Size-Dependent Localization and Penetration of Ultrasmall Gold Nanoparticles in Cancer Cells, Multicellular Spheroids, and Tumors *in Vivo*. *ACS Nano* **2012**, *6***,** 4483-4493.

18. Chou, L.Y.T.; Zagorovsky, K.; Chan, W.C. DNA Assembly of Nanoparticle Superstructures for Controlled Biological Delivery and Elimination. *Nat. Nanotechnol*. **2014**, *9*, 148-155.

19. Blanco, E.; Shen, H.; Ferrari, M. Principles of Nanoparticle Design for Overcoming Biological Barriers to Drug Delivery. *Nat. Biotechnol*. **2015,** *33*, 941-951.

20. Irvine, D.J.; Hanson, M.C.; Rakhra, K.; Tokatlian, T. Synthetic Nanoparticles for Vaccines and Immunotherapy. *Chem. Rev*. **2015**, *115*, 11109-11146.

21. Veiseh, O.; Doloff, J.C.; Ma, M.; Vegas, A.J.; Tam, H.H.; Bader, A.R.; Li, J.; Langan, E.; Wyckoff, J.; Loo, W.S.; Jhunjhunwala, S.; Chiu, A.; Siebert, S.; Tang, K.; Hollister-Lock, J.; Aresta-Dasilva, S.; Bochenek, M.; Mendoza-Elias, J.; Wang, Y.; Qi, M.; *et al*. Size- and Shape-Dependent Foreign Body Immune Response to Materials Implanted in Rodents and Non-Human Primates. *Nat. Mater*. **2015**, *14*, 643-651.

22. Grassian, V.H.; Haes, A.J.; Mudunkotuwa, I.A.; Demokritou, P.; Kane, A.B.; Murphy, C.J.; Hutchison, J.E.; Isaacs, J.A.; Jun, Y.S.; Karn, B.; Khondaker, S.I.; Larsen, S.C.; Lau,

B.L.T.; Pettibone, J.M.; Sadik, O.A.; Saleh, N.B.; Teague, C. NanoEHS - Defining Fundamental Science Needs: No Easy Feat When the Simple Itself Is Complex. *Environ. Sci.: Nano*. **2016**, *3*, 15-27.

23. Hamad-Schifferli, K. Exploiting the Novel Properties of Protein Coronas: Emerging Applications in Nanomedicine. *Nanomedicine* **2015**, *10*, 1663-1674.

24. Malvindi, M.A.; Brunetti, V.; Vecchio, G.; Galeone, A.; Cingolani, R.; Pompa, P.P. SiO_2 Nanoparticles Biocompatibility and Their Potential for Gene Delivery and Silencing. *Nanoscale* **2012**, *4*, 486-495.

25. Sokolova, V.; Westendorf, A.M.; Buer, J.; Uberla, K.; Epple, M. The Potential of Nanoparticles for the Immunization Against Viral Infections. *J. Mater. Chem. B.* **2015**, *3*, 4767-4779.

26. Zhang, Y.N.; Poon, W.; Tavares, A.J.; McGilvray, I.D.; Chan, W.C. Nanoparticle–Liver Interactions: Cellular Uptake and Hepatobiliary Elimination. *J. Controlled Release*. **2016**, *240*, 332-348.

27. Hadjidemetriou, M.; Al-Ahmady, Z.; Mazza, M.; Collins, R.F.; Dawson, K.A.; Kostarelos, K. *In Vivo* Biomolecule Corona around Blood-Circulating, Clinically Used and Antibody-Targeted Lipid Bilayer Nanoscale Vesicles. *ACS Nano* **2015**, *9*, 8142-8156.

28. Walczyk, D.; Bombelli, F.B.; Monopoli, M.P.; Lynch, I.; Dawson, K.A. What the Cell "Sees" in Bionanoscience. *J. Am. Chem. Soc.* **2010**, *132*, 5761-5768.

29. Walkey, C.D.; Olsen, J.B.; Song, F.; Liu, R.; Guo, H.; Olsen, D.W.; Cohen, Y.; Emili, A.; Chan, W.C. Protein Corona Fingerprinting Predicts the Cellular Interaction of Gold and Silver Nanoparticles. *ACS Nano* **2014**, *8*, 2439-2455.

30. Kelly, P.M.; Åberg, C.; Polo, E.; O'Connell, A.; Cookman, J.; Fallon, J.; Krpetić, Ž.; Dawson, K.A. Mapping Protein Binding Sites on the Biomolecular Corona of Nanoparticles. *Nat. Nanotechnol*. **2015**, *10*, 472-479.

31. Lo Giudice, M.C.; Herda, L.M.; Polo, E.; Dawson, K.A. *In Situ* Characterization of Nanoparticle Biomolecular Interactions in Complex Biological Media by Flow Cytometry *Nat. Commun*. **2016**, *7*, 13475.

32. Huhn, J.; Fedeli, C.; Zhang, Q.; Masood, A.; del Pino, P.; Khashab, N.M.; Papini, E.; Parak, W.J. Dissociation Coefficients of Protein Adsorption to Nanoparticles as Quantitative Metrics for Description of the Protein Corona: A Comparison of Experimental Techniques and Methodological Relevance. *Int. J. Biochem. Cell Biol.* **2016**, *75*, 148-161.

33. Kumar, V.; Butcher, S.J.; Öörni, K.; Engelhardt, P.; Heikkonen, J.; Kaski, K.; Ala-Korpela, M.; Kovanen, P.T. Three-Dimensional CryoEM Reconstruction of Native LDL Particles to 16Å Resolution at Physiological Body Temperature. *PLoS ONE* **2011**, *6*, e18841.

34. Mora, S.; Szklo, M.; Otvos, J.D.; Greenland, P.; Psaty, B.M.; Goff, D.C. Jr.; O'Leary, D.H.; Saad, M.F.; Tsai, M.Y.; Sharrett, A.R. LDL Particle Subclasses, LDL Particle Size, and Carotid Atherosclerosis in the Multi-Ethnic Study of Atherosclerosis (MESA). *Atherosclerosis* **2007**, *192*, 211-217.

35. Segrest, J.P.; Jones, M.K.; De Loof, H.; Dashti, N. Structure of Apolipoprotein B-100 in Low Density Lipoproteins. *J. Lipid Res*. **2001**, *42*, 1346-1367.

36. Hansel, T.T.; Kropshofer, H.; Singer, T.; Mitchell, J.A.; George, A.J.T. The Safety and Side Effects of Monoclonal Antibodies. *Nat. Rev. Drug Discovery*. **2010**, *9*, 325-338.

37. Herda, L.M.; Hristov, D.R.; Lo Giudice, M.C.; Polo, E.; Dawson, K.A. Mapping of Molecular Structure of the Nanoscale Surface in Bionanoparticles. *J. Am. Chem. Soc*. **2017,** *139*, 111-114.

38. Resch-Genger, U.; Grabolle, M.; Cavaliere-Jaricot, S.; Nitschke, R.; Nann, T. Quantum Dots *Versus* Organic Dyes as Fluorescent Labels. *Nat. Methods* **2008**, *5***,** 763-775.

39. Zarschler, K.; Prapainop, K.; Mahon, E.; Rocks, L.; Bramini, M.; Kelly, P.M.; Stephan, H.; Dawson, K.A. Diagnostic Nanoparticle Targeting of the EGF-Receptor in Complex Biological Conditions Using Single-Domain Antibodies. *Nanoscale* **2014**, *6***,** 6046-6056.

40. Levitan, I.; Volkov, S.; Subbaiah, P.V. Oxidized LDL: Diversity, Patterns of Recognition, and Pathophysiology. *Antioxid. Redox Signaling* **2010**, *13,* 39-75.

41. Brown, M.S.; Goldstein, J.L. Reversible Accumulation of Cholesteryl Esters in Macrophages Incubated with Acetylated Lipoproteins. *J. Cell Biol*. **1979**, *82*, 597-613.

42. Karsten, C.M.; Köhl, J. The Immunoglobulin, IgG Fc Receptor and Complement Triangle in Autoimmune Diseases. *Immunobiology* **2012**, *217*, 1067-1079.

43. Lund, J.; Winter, G.; Jones, P.T.; Pound, J.D.; Tanaka, T.; Walker, M.R.; Artymiuk, P.J.; Arata, Y.; Burton, D.R.; Jefferis, R.; Woof, J.M. Human Fc Gamma RI and Fc Gamma RII Interact with Distinct but Overlapping Sites on Human IgG. *J. Immunol*. **1991**, *147*, 2657-2662.

44. Canfield, S.M.; Morrison, S.L. The Binding Affinity of Human IgG for Its High Affinity Fc Receptor Is Determined by Multiple Amino Acids in the CH2 Domain and Is Modulated by the Hinge Region. *J. Exp. Med*. **1991**, *173*,1483-1491.

45. Hristov, D.R.; Mahon, E.; Dawson, K.A. Controlling Aqueous Silica Nanoparticle Synthesis in the 10-100 nm Range. *Chem. Commun*. **2015**, *51*, 17420-17423.

46. Piella, J.; Bastús, N.G.; Puntes, V. Size-Controlled Synthesis of Sub-10-Nanometer Citrate-Stabilized Gold Nanoparticles and Related Optical Properties. *Chem. Mater*. **2016,** *28*, 1066-1075.

47. Gallo, J.; García, I.; Genicio, N.; Penadés, S. CdTe-Based QDs: Preparation, Cytotoxicity, and Tumor Cell Death by Targeting Transferrin Receptor. *Part. Part. Syst. Charact.* **2014**, *31,* 126-133.

TOC